REPORT-NO

Advanced Steam-Electric Power Cycle for Advanced Reactor Concepts

September 2020

David Andrs
Lise C. Charlot
Jack M. Cavaluzzi

Changing the World's Energy Future

INL is a U.S. Department of Energy National Laboratory operated by Battelle Energy Alliance, LLC

REPORT-NO

Advanced Steam-Electric Power Cycle for Advanced Reactor Concepts

David Andrs
Lise C. Charlot
Jack M. Cavaluzzi

September 2020

Idaho National Laboratory
Idaho Falls, Idaho 83415

http://www.inl.gov

Prepared for the
U.S. Department of Energy
Office of Nuclear Energy
Under DOE Idaho Operations Office
Contract DE-AC07-05ID14517

Page intentionally left blank

ABSTRACT

This report presents improvements made to RELAP-7 for modeling Rankine power cycles, which are used on the secondary side of some advanced reactor concepts. For example, for a High-Temperature gas-cooled Reactor Pebble bed Module (HTR-PM), in the primary loop, helium transfers heat from the fuel to a steam generator, and on the secondary side, dry steam from the steam generator applies work to a turbine, which is converted into electrical power by a generator. After passing through the turbine, the steam passes through a condenser and pumped to the steam generator inlet, completing a Rankine cycle on the secondary side. This HTR-PM concept is used as an example to demonstrate a steam-electric power cycle capability in RELAP-7.

This power cycle requires a number of different physical components, including a pump, compressor, turbine, steam generator, and condenser. The steam generator is modeled using a heat exchange between primary and secondary loops, and the condenser is modeled using a cooling source term. Recent efforts demonstrated preliminary models for the turbomachinery components (pump/compressor and turbine), but more physical models were required. Furthermore, several improvements were made for the robustness of mixed single-phase/two-phase flow present in a Rankine cycle.

CONTENTS

1 INTRODUCTION

This report presents improvements made to RELAP-7 for modeling Rankine power cycles, which are used on the secondary side of some advanced reactor concepts. For example, for a High-Temperature gas-cooled Reactor Pebble bed Module (HTR-PM), in the primary loop, helium transfers heat from the fuel to a steam generator, and on the secondary side, dry steam from the steam generator applies work to a turbine, which is converted into electrical power by a generator. After passing through the turbine, the steam passes through a condenser and pumped to the steam generator inlet, completing a Rankine cycle on the secondary side. This HTR-PM concept is used as an example to demonstrate a steam-electric power cycle capability in RELAP-7.

This power cycle requires a number of different physical components, including a pump, compressor, turbine, steam generator, and condenser. The steam generator is modeled using a heat exchange between primary and secondary loops, and the condenser is modeled using a cooling source term. Recent efforts demonstrated preliminary models for the turbomachinery components (pump/compressor and turbine)[1], but more physical models were required. Furthermore, several improvements were made for the robustness of mixed single-phase/two-phase flow present in a Rankine cycle.

This report is organized as follows. Section 2 describes the model improvements made to RELAP-7, which include improvements made to the two-phase flow model, closures, and component models. Section 3 presents results from some numerical experiments made with a HTR-PM system using RELAP-7, and Section 4 gives some conclusions.

2 MODELS

This section describes the improvements that were made in physical models to enable modeling of steam-electric cycle.

2.1 Phase Appearance and Disappearance

Phase appearance and disappearance is a very important capability of a two-phase flow solver. It allows the simulation to run in "single-phase" regime while still tracking the two phases, but having them not interact with each other.

This section describes the modifications implemented in RELAP-7 to enable the code to run in this "single-phase" regime.

2.1.1 Volume Fraction Mapper

Volume fraction mapper is a mechanism in RELAP-7 that limits the volume fraction of a phase between 0 and 1. This is important for numerical stability of the two-phase solver.

The idea behind the remapper is that we solve for an auxiliary variable β which can attain values from $-\infty$

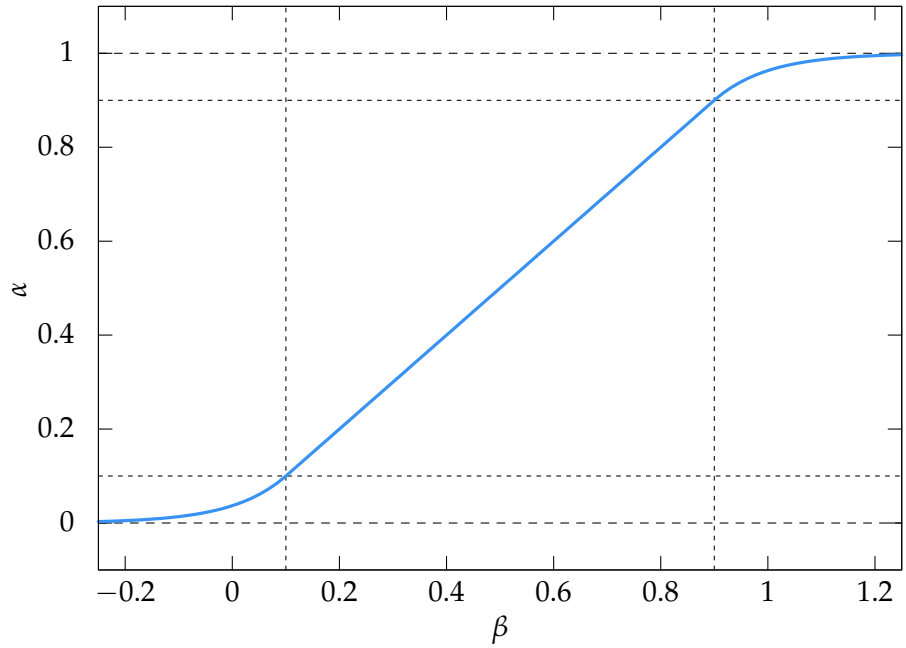

Figure 1: Example of volume fraction remapping from 0.1 to 0.9

to $+\infty$. This value is then remapped into an interval $(0,1)$. The mapping is divided into 3 regions: 1 linear region where $\Delta\beta = \Delta\alpha$ and 2 exponential regions where large change in β results in small change in α. It is important to note that the resulting mapping is smooth so that it does not create difficulties for the underlying non-linear solver. By default, the lower and upper limit of vapor volume fraction is 1×10^{-6} and 9.99999×10^{-1}. Users can specify the lower and upper point where the function transitions from exponential region to the linear region and linear region to exponential region, respectively.

2.1.2 Flow Map Modifications

To properly handle the phase appearance and disappearance, two additional flow regimes were added to the internal flow map: (1) pure liquid, and (2) pure vapor. In those regimes, the model will turn off all phase interaction and each phase will behave independently of the other one. This independent behavior is not however fully independent. Some small amount of dependency is maintained to prevent difficulties when transitioning from the single-phase regime into the two-phase one (see section 2.1.3 for further details).

By default, α_{lower} and α_{upper} are set to 1×10^{-4} and 9.999×10^{-1}, respectively.

2.1.3 Weighting Function for Transition to and from Single Phase Regimes

The transition from single-phase region into the two-phase region and back should not happen suddenly as in using a step function. This would have a detrimental effect on the underlying non-linear solver. Thus, a third order polynomial transition is used to go from 0 to 1. The transition from pure liquid starts at $\alpha_m in$ (which is the lower limit specified by a user and corresponds to the point where the volume fraction remapper goes

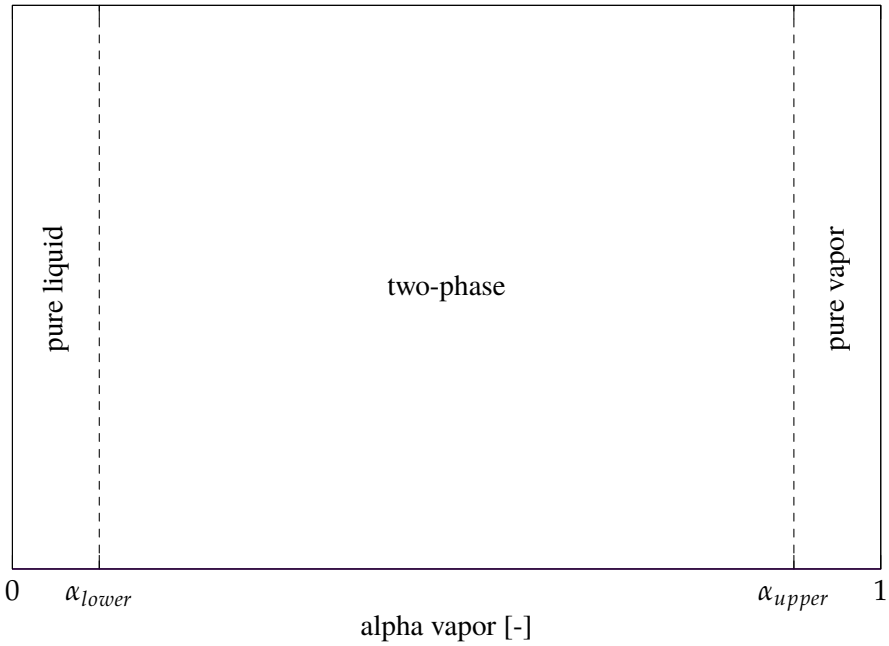

Figure 2: Flow regime map

from the lower exponential region to the linear region) and ends at α_{lower}. The transition from two-phase region to pure vapor region starts at α_{upper} and ends at α_{max} (which is the upper limit specified by an user and corresponds to the point where the volume fraction remapper goes from the linear region into the upper exponential region).

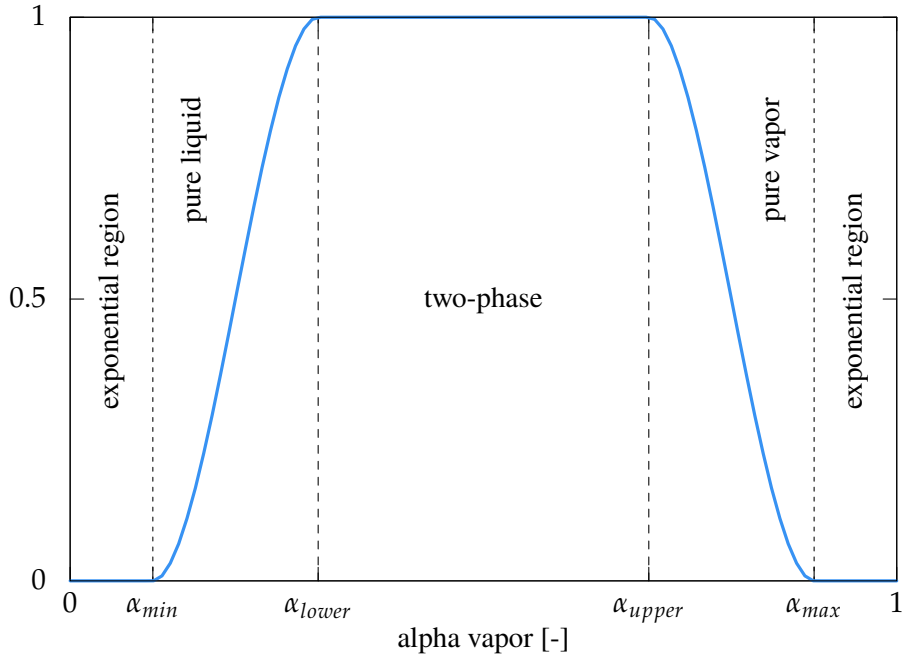

Figure 3: Weighting function for transition between single- and two-phase regime

The transition function is depicted on Figure 3, α_{min} and α_{max} are user specified bounds, α_{lower} and α_{upper} are set to 1×10^{-4} and 9.999×10^{-1}, respectively. Note the figure is not to scale to better show the transition function.

2.1.4 Specific Interfacial Area

Specific interfacial area curve was modified such that the lower value specified by the user is specified at the transition from the single-phase region to the two-phase region and vice versa.

The curve in the single phase region was designed to have continuous derivative (to prevent numerical issues in the underlying non-linear solver) at the transition to and from the single-phase region and being zero for $\alpha = 0$ and 1.

Note that is is important for the curve to be non-negative at all points.

Figure 4 shows the modified specific interfacial area curve.

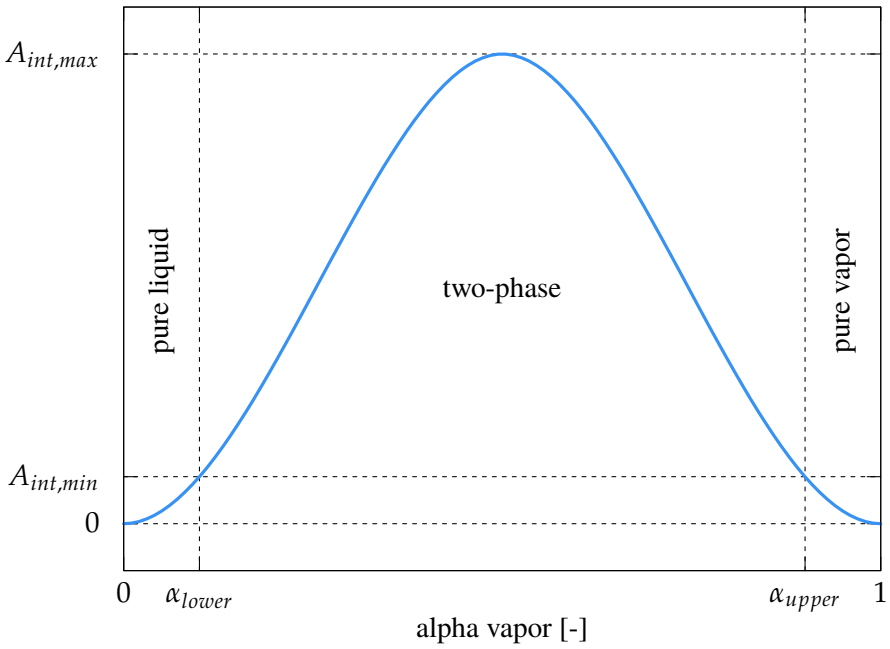

Figure 4: Specific interfacial area curve

2.1.5 Acoustic Impedance Modification

The following modifications are applied to liquid and vapor acoustic impedance:

$$Z_{\text{liq}} = \begin{cases} wt * Z_L & \text{in single-phase region} \\ Z_L & \text{in two-phase region} \end{cases} \tag{1}$$

$$Z_{\text{vap}} = \begin{cases} wt * Z_V & \text{in single-phase region} \\ Z_V & \text{in two-phase region} \end{cases} \tag{2}$$

where wt is the weighting function described in section 2.1.3, Z_L is the liquid acoustic impedance computed as $Z_L = \rho_{\text{liq}} \cdot c_{\text{liq}}$ and Z_V is the vapor acoustic impedance computed as $Z_V = \rho_{\text{vap}} \cdot c_{\text{vap}}$.

Then, the following interfacial quantities are using the modified values:

$$\bar{p}_{\text{int}} = \frac{(Z_{\text{vap}} \cdot p_{\text{liq}} + Z_{\text{liq}} \cdot p_{\text{vap}})}{Z_{\text{liq}} + Z_{\text{vap}}} \tag{3}$$

$$\bar{v}_{\text{int}} = \frac{Z_{\text{liq}} * v_{\text{liq}} + Z_{\text{vap}} \cdot v_{\text{vap}}}{Z_{\text{liq}} \cdot Z_{\text{vap}}} \tag{4}$$

$$p_{\text{int}} = \bar{p}_{\text{int}} + \frac{Z_{\text{vap}} \cdot Z_{\text{liq}}}{Z_{\text{vap}} + Z_{\text{liq}}} \cdot \text{sign}\left(\frac{\partial \alpha_{\text{liq}}}{\partial x}\right) \cdot (v_{\text{vap}} - v_{\text{liq}}) \tag{5}$$

$$v_{\text{int}} = \bar{v}_{\text{int}} + \text{sign}\left(\frac{\partial \alpha_{\text{liq}}}{\partial x}\right) \cdot \frac{p_{\text{vap}} - p_{\text{liq}}}{Z_{\text{liq}} + Z_{\text{vap}}} \tag{6}$$

2.1.6 Pressure Relaxation Modification

The pressure relaxation closure was modified as such

$$\mu = wt \cdot \frac{A_{\text{int}}}{Z_{\text{liq}} + Z_{\text{vap}}} \tag{7}$$

where wt is the weighing function described in the section 2.1.3 and Z_{liq} and Z_{vap} are acoustic impedances computed as described in section 2.1.5. Several test runs showed that using only the modified acoustic impedances is not strong enough to turn interfacial interaction, therefore the weighting function was additionally applied.

2.1.7 Velocity Relaxation Modification

No modification was needed for the velocity relaxation closure correlation, since

$$\lambda = \frac{1}{3} \cdot \mu \cdot Z_{\text{liq}} \cdot Z_{\text{vap}} \tag{8}$$

so the acoustic impedance modification (section 2.1.5) and pressure relaxation modification (section 2.1.6) automatically affects the velocity relaxation coefficient and turn the needed interaction off.

2.2 Interfacial Friction Closure

A closure for interfacial friction only exists in TRACE closure set. If using simple closure set, only a constant value can be prescribed by an user. In that case the computation has the following form:

$$f_{\text{int}} = wt \cdot const \tag{9}$$

where wt is the weighing function described in the section 2.1.3 and $const$ is the user prescribed value. This effectively turn off the interfacial friction for the single-phase regions. This change was needed, since the interfacial friction term does not include A_{int}, thus the interaction has to be handled by the weighting function.

2.3 Interfacial Heat Transfer Coefficient Closure

Interfacial heat transfer coefficient can be either specified by an user or computed by a closure correlation. In both cases, the way it is computed was not modified, because the phase interaction is determined by A_{int}. Let us review the interfacial heat transfer term

$$htc_{\text{int}} \cdot A_{\text{int}} \cdot A \cdot (T_{\text{int}} - T_k) \tag{10}$$

Refer to section 2.1.4 to see how specific interfacial area would make this term small and therefore turn of the phase interaction int he single phase region.

2.3.1 Flashing Model

The flashing model was adopted from TRACE[2]. The model is invoked when liquid temperature is above saturation temperature. The already computed interfacial heat transfer coefficient is modified by adding the following quantity

$$htc_{\text{int,liq,flash}} = 1 \times 10^7 \cdot \alpha_{\text{liq}} \cdot \max\{0.1, \min\{20, 20 \cdot (T_{\text{liq}} - T_{\text{sat}})\}\} \tag{11}$$

2.4 Wall Boiling Model

The wall heat flux is partitioned into a portion which may go directly to convective heat transfer to the vapor phase and a portion which is available to both convectively heat the liquid phase and generate vapor via wall boiling. This partitioning is specified with a simple function κ. The portion of the wall heat flux available to convectively heat the liquid phase and generate vapor is further partitioned into a portion which may convectively heat the liquid phase and a portion which goes toward generation of vapor. This partitioning is specified with a simple function f_{boil}. Rendering this into equation form,

$$q_{\text{wall,total}} = q^{\text{conv}}_{\text{wall}\to\text{liq}} + q^{\text{boil}}_{\text{wall}\to\text{liq}} + q_{\text{wall}\to\text{vap}}\,, \tag{12}$$

$$q^{\text{boil}}_{\text{wall}\to\text{liq}} = f_{\text{boil}}\, h_{\text{wall,liq}}\,(T_{\text{wall}} - T_{\text{liq}})\,\kappa\,, \tag{13}$$

$$q^{\text{conv}}_{\text{wall}\to\text{liq}} = (1 - f_{\text{boil}})\, h_{\text{wall,liq}}(T_{\text{wall}} - T_{\text{liq}})\,\kappa\,, \tag{14}$$

$$q_{\text{wall}\to\text{vap}} = h_{\text{wall,vap}}\,(T_{\text{wall}} - T_{\text{vap}})(1 - \kappa)\,. \tag{15}$$

The mass flux of vapor generated by boiling at the wall due to wall heat flux is

$$\Gamma^{\text{wall}}_{\text{liq}\to\text{vap}} = \frac{q^{boil}_{\text{wall}\to\text{liq}}}{h^{\text{int}}_{\text{vap}} - h_{\text{liq}}}\,, \tag{16}$$

where $h^{\text{int}}_{\text{vap}} - h_{\text{liq}}$ represents the change in specific enthalpy required for vaporization.

Changes have been made to the calculation of the wall boiling fraction f_{boil} and to the heat flux partitioning κ to capture the boiling phenomena more accurately. The previous model was comparing the wall temperature to the liquid saturation temperature to trigger boiling without accounting for the liquid temperature. To better capture subcooled boiling, a temperature of onset of nucleate boiling is introduced.

2.4.1 Temperature of Onset of Nucleate Boiling

The temperature of onset of nucleate boiling from TRACE [2] is used. The wall temperature for onset of nucleate boiling is modeled as

$$T_{\text{ONB}} = T_{\text{liq}} + \frac{1}{4}\left(\sqrt{\Delta T_{\text{ONB,sat}}} + \sqrt{\Delta T_{\text{ONB,sat}} + 4\,\Delta T_{\text{sub}}}\right)^2\,, \tag{17}$$

in which ΔT_{sub} is the liquid phase subcooling temperature:

$$\Delta T_{\text{sub}} = T_{\text{sat}} - T_{\text{liq}}\,, \tag{18}$$

and $\Delta T_{\text{ONB,sat}}$ is the wall superheat necessary for the onset of nucleate boiling when the liquid is at saturation temperature, defined as

$$\Delta T_{\text{ONB,sat}} = \frac{2\,h_{\text{FC}}\,\sigma\,T_{\text{sat}}}{F^2(\phi)\,\rho_{\text{vap}}\,h_{\text{lat}}\,k_{\text{liq}}}\,. \tag{19}$$

In this equation, h_{FC} is the two-phase flow forced-convection wall heat transfer coefficient; $F(\phi)$ is the contact angle correction factor:

$$F(\phi) = 1 - \exp\left(-\phi^3 - 0.5\,\phi\right)\,. \tag{20}$$

In this model, ϕ is fixed to 38°.

2.4.2 Wall boiling fraction

The wall boiling fraction is modified to use T_{ONB} as a threshold to generate vapor at the wall:

$$\begin{aligned} T_{wall} \le T_{\text{ONB}} \quad &\Rightarrow \quad f_{\text{boil}} = 0 \\ T_{wall} > T_{\text{ONB}} \quad &\Rightarrow \quad f_{\text{boil}} = 1 - e^{-0.25(T_{\text{wall}} - T_{\text{ONB}})} \end{aligned} \tag{21}$$

The wall boiling fraction is shown as a function of the wall temperature in figure 5.

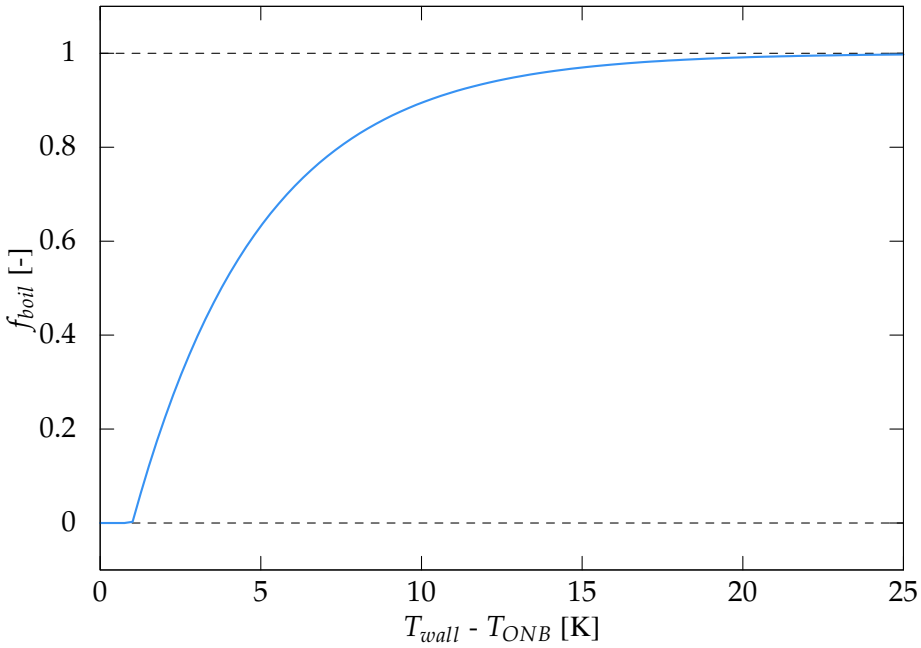

Figure 5: Boiling fraction curve

2.4.3 Heat Flux Partitioning

The heat flux partition can be seen as the fraction of liquid in contact with the wall. It is assumed that as the void fraction increases, the flow regime transitions from bubbly flow to slug and churn flow and to annular/droplet flow. With this assumption, liquid is in contact with the wall up to very high void fractions where the liquid film vanishes and the vapor phase get in contact with the wall. This transition is assumed to happen between void fractions of 0.95 and 0.97. Thus, κ is equal to 1 when the void fraction is below 0.95 and κ is set to 0 when the void fraction is above 0.97. A third order polynomial is used to make a smooth transition as shown in figure 6b.

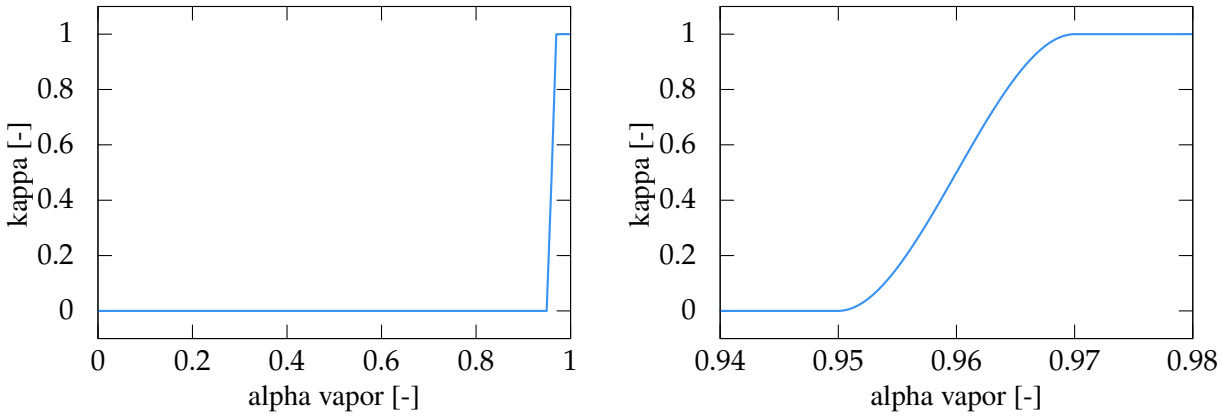

(a) Heat flux partitioning vs vapor volume fraction **(b)** Detail of the transition from pure liquid to pure vapor

Figure 6: Heat flux partitioning

2.5 Shaft

This component implements a shaft used to connect components such as a turbine, pump, and motor. The shaft provides a rigid connection between connected components, thus there is only one rotational speed shared by all connections. The shaft receives torque and inertia coupled variables from the components connected to it. The angular speed of the shaft and connected components is dictated by the torque-inertia balance,

$$\sum_{k=1}^{n} I_k \frac{d\omega}{dt} = \sum_{k=1}^{n} \tau_k \,, \tag{22}$$

where

- ω is the angular speed of the shaft and all connected components,
- I_k is the moment of inertia for the k^{th} connection,
- τ_k is the net torque for the k^{th} connection, and
- n is the number of components connected to the shaft.

2.6 Pump

The pump model relies on homologous pump curves to compute the pressure head (H) and hydraulic torque (τ_H) as a function of the flow rate into the pump (Q) and the pump rotational speed (ω). In conventional homologous pump formulation, non-dimensional ratios α, ν, h, and t are formed as:

$$\alpha = \left(\frac{\omega}{\omega_R}\right) \tag{23}$$

$$\nu = \left(\frac{Q}{Q_R}\right) \tag{24}$$

$$h = \left(\frac{H}{H_R}\right) \tag{25}$$

$$t = \left(\frac{\tau_H}{\tau_{H,R}}\right) \tag{26}$$

where ω_R, Q_R, H_R, and $\tau_{H,R}$ are rated pump speed, rated pump volumetric flow, rated pressure head, and rated hydraulic torque, respectively.

This model employees the polar homologous representation so that all octants of pump performance can be ordered with respect to a single independent variable. The independent variable for polar homologous pump curves is:

$$x = C + \tan^{-1}\left(\frac{\alpha}{\nu}\right) \tag{27}$$

The constant C assumes different values depending on the mode of pump operation.

The pump is said to be operating in the "α range" if $|\frac{\nu}{\alpha}| \leq 1$, and it is operating in the "ν range" otherwise.

The dependent variables are head and torque functions, WH and WT, which are defined as:

$$WH = \left(\frac{h}{\alpha^2}\middle|\frac{h}{\nu^2}\right) \Big/ \left(1+\left(\left(\frac{\nu}{\alpha}\right)^2\right)\middle|\left(\frac{\alpha}{\nu}\right)^2\right) \tag{28}$$

$$WT = \left(\frac{t}{\alpha^2}\middle|\frac{t}{\nu^2}\right) \Big/ \left(1+\left(\left(\frac{\nu}{\alpha}\right)^2\right)\middle|\left(\frac{\alpha}{\nu}\right)^2\right) \tag{29}$$

Where (|) represents a decision with left and right corresponding to α and ν ranges, respectively.

The net torque delivered from the pump to the shaft is the sum of hydraulic and frictional torques $\tau = \tau_H + \tau_{fr}$.

The pump moment of inertia is modeled with a polynomial in the quantity $|\frac{\omega}{\omega_R}|$, according to:

$$I_{\text{pump}} = \begin{cases} I_{const} & \text{if } |\frac{\omega}{\omega_R}| < S_{cr} \\ I_{p0} + I_{p1}|\frac{\omega}{\omega_R}| + I_{p2}|\frac{\omega}{\omega_R}|^2 + I_{p3}|\frac{\omega}{\omega_R}|^3 & \text{if } |\frac{\omega}{\omega_R}| \geq S_{cr} \end{cases} \tag{30}$$

The user specifies the coefficients and critical speed ratio S_{cr}, below which the inertia is constant.

The pump frictional torque is modeled as:

$$\tau_{fr} = -\tau_f|\frac{\omega}{\omega_R}|^2 \tag{31}$$

Momentum and energy source terms are added to the pump volume vapor momentum and energy conservation equations.

$$S_{momentum,\text{vap}} = \rho_{\text{vap}} g H A_{\text{pump}} \tag{32}$$

$$S_{energy,\text{vap}} = \tau\omega \tag{33}$$

2.7 Turbine

The shaft model described in section 2.5 allows to connect multiple turbines to a shaft to model a multi stage turbine. The power P_k to be extracted by the k^{th} stage is prescribed by the user. The net torque is calculated by:

$$\tau_k = \frac{P_k}{\omega} - C_{b,k}\frac{\omega|\omega|}{\omega_R^2} \tag{34}$$

where $C_{b,k}$ is the bearing and windage frictional coefficient and ω_R^2 is the rated shaft speed. The moment of inertia is provided by the user.

Momentum and energy source terms are added to the turbine volume momentum and energy conservation equations.

$$S_{momentum,\text{vap}} = -\frac{P_k}{u} \tag{35}$$

$$S_{energy,\text{vap}} = -P_k \tag{36}$$

2.8 PID Controller

The control system is an important part of the secondary loop as it helps maintaining stable flow conditions in the loop. Thus, a simple control system has been implemented and includes a PID (proportional–integral–derivative) controller. A setpoint X_0 is defined for a variable of the system $X(t)$. The error $e(t)$ between the setpoint and the current value is calculated. Then the control variable Y is calculated by:

$$\begin{aligned} e(t) &= X_0 - X(t) \\ Y(t) &= K_p e(t) + K_i \int_0^t e(t')dt' + K_d \frac{de}{dt}(t)\,, \end{aligned} \tag{37}$$

where K_p is the proportional gain, K_i is the integral gain and K_d the derivative gain. These are positive coefficients provided by the user as they strongly depend on the behavior of the system.

3 RESULTS

The RELAP-7 model and components are shown on figure 7.

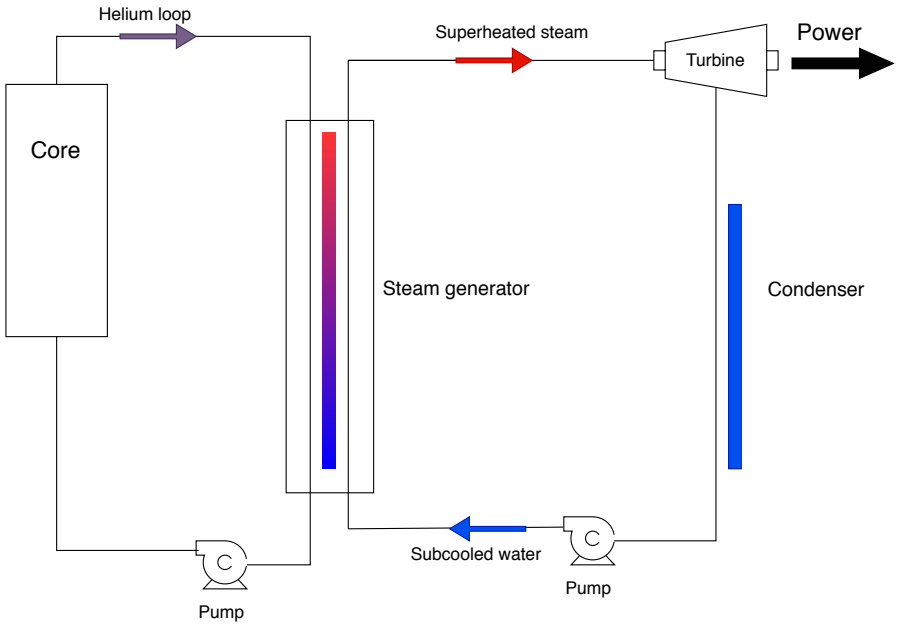

Figure 7: RELAP-7 Model of HTR-PM

This section shows results and parameters for relevant parts of the secondary side.

3.1 Steam Generator

The parameters of the steam generator are listed in Table 1.

Table 1: Parameters of steam generator

General		
Length	8.2	m
Cross-sectional area	0.19635	m^2
Wall thickness	3.775	mm
Primary side		
Inlet temperature	593	K
Outlet temperature	964	K
Outlet pressure	7	MPa
Total mass flow rate	96	kg/s
Total heat transfer area	3074	m^2
Secondary side		
Total mass flow rate	186	kg/s
Inlet liquid temperature	578.15	K
Outlet vapor temperature	668	K
Outlet pressure	13.249	MPa
Heat transfer coefficient liquid	5,000	W/m^2
Heat transfer coefficient vapor	300	W/m^2
Total heat transfer area	5571	m^2

On the primary side, heat was removed from the helium resulting in a 371 K temperature drop for the helium. The temperature and void fraction distribution on the secondary side on shown in Figure 8.

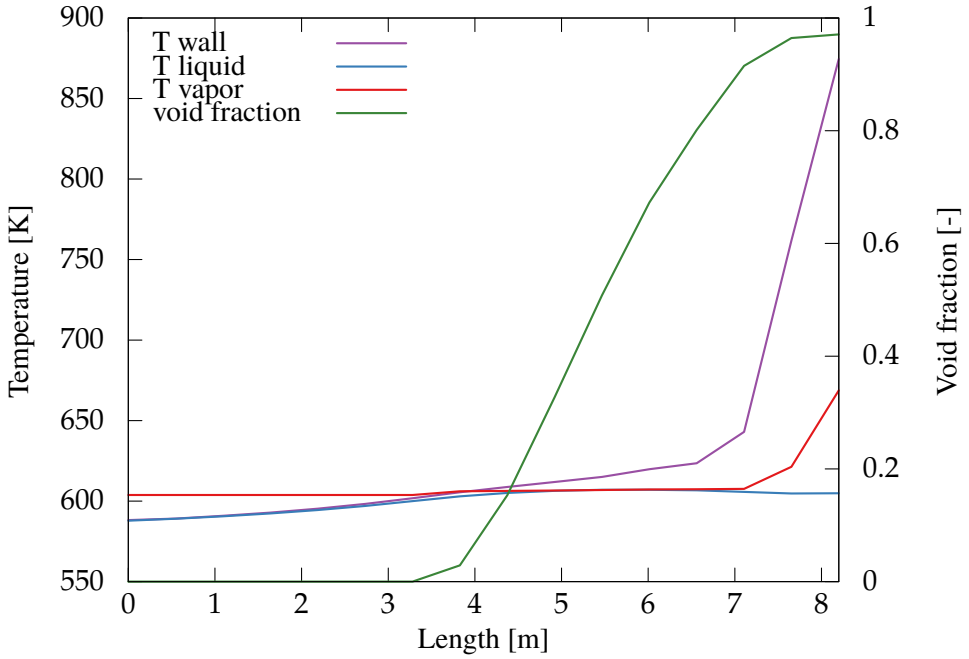

Figure 8: Temperature and void distribution in the secondary side of the steam generator

Subcooled liquid water is heated up to saturation, steam is generated and as void fraction approaches 1, the steam temperature rises above the saturation temperature.

3.2 Pump

A simple pump simulation was ran to demonstrate the pressure rise produced by the pump model. The parameters of the pump for this simulation are listed in Table 2. Homologous pump head and torque curves for a Bingham centrifugal pump were used in this simulation.

Table 2: Parameters of pump

General		
Omega rated, ω_R	900	rpm
Torque rated, τ_R	50	N/m
Head rated, H_R	840	m
Volumetric flow rated, Q_R	0.202	m^3/s
Friction torque coefficient, τf	10	[-]
Constant inertia, I_{const}	20	$kg \cdot m^2$

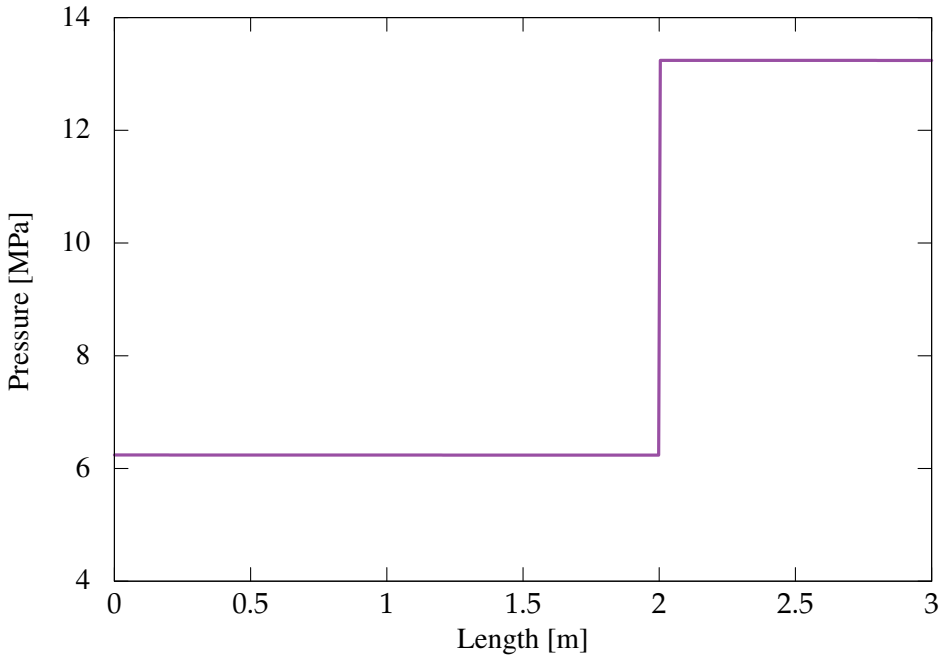

Figure 9: Liquid pressure across the pump

3.3 Turbine

A two-stage turbine is used to extract power from the super heated steam exiting the steam generator. The parameters for the high pressure (HP) stage and low pressure (LP) stage are given in Table 3. The total power extracted by this two-stage tubine is 147MW. The final shaft speed is 455 rad/s. The pressure and temperature across the turbine are shown on Figure 10.

Table 3: Parameters of 2 stage turbine

	HP stage		LP stage	
Omega rated, ω_R	800	rad/s	800	rad/s
Friction coefficient, C_b	500,000	N·m	500,000	N·m
Moment of inertia, I	50,000	kg·m^2	100,000	kg·m^2
Power, P	97	MW	5	MW

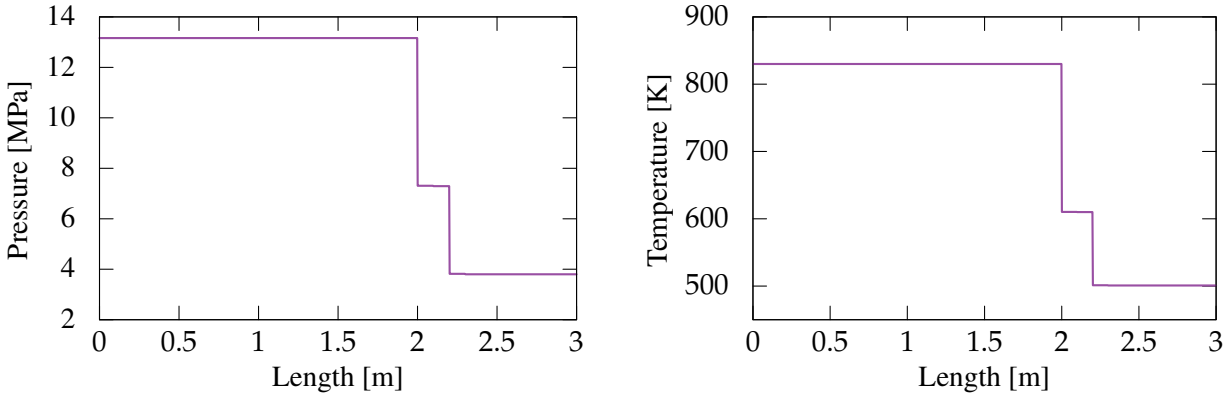

(a) **(b)**

Figure 10: Vapor Pressure (a) and vapor temperature (b) across the 2 stage turbine

4 CONCLUSIONS

A Rankine cycle was modeled using RELAP-7. The improvements made to properly model phase appearance/disappearance allowed to run robustly in the single phase regime and the transition to the two-phase regime. This allowed to successfully simulate the steam generator which has subcooled water at the inlet and generates dry superheated steam. The improved turbo-machinery models allow to properly model a pump or turbine and the associated shaft and are compatible with the 7-equation model, even if they operate only in single phase regime.

REFERENCES

[1] D. Andrs, R. A. Berry, J. M. Cavaluzzi, L. Charlot, J. E. Hansel, and R. C. Martineau, "Power Generation Cycle with RELAP-7," Tech. Rep. INL/EXT-20-57890, Idaho National Engineering Laboratory, 3 2020.

[2] N. TRACE, "V5. 0 theory manual: Field equations," *Solution Methods, and Physical Models (Washington: United States Nuclear Regulatory Commission)*, 2010.